

**Oxidative coupling of aniline and desulphurization over
nitrogen rich mesoporous carbon**

Journal:	<i>Catalysis Science & Technology</i>
Manuscript ID:	CY-ART-04-2015-000484.R1
Article Type:	Paper
Date Submitted by the Author:	30-Apr-2015
Complete List of Authors:	Goyal, Reena; CSIR-IIP, Dehradun, Dumbre, Deepa; RMIT, Department of Applied Chemistry, RMIT University, Melbourne-3001 (Australia) L. N., Konathala; Indian Institute of Petroleum, Analytical Sciences Pandey, Monica; CSIR-IIP, Dehradun, Bordoloi, Ankur; CSIR-IIP,

ARTICLE

Oxidative coupling of aniline and desulphurization over nitrogen rich mesoporous carbon

Cite this: DOI: 10.1039/x0xx00000x

Reena Goyal,^a Deepa Dumbre,^b L. N. Sivakumar Konathala,^a Monica Pandey,^a and Ankur Bordoloi^{*a}

Received 00th January 2012,
Accepted 00th January 2012

DOI: 10.1039/x0xx00000x

www.rsc.org/

Tungsten loaded mesoporous nitrogen rich carbon (WO_xMCN_x) materials were synthesized using SBA-15 as hard template. With these new multifunctional materials, we performed a one-pot oxidative coupling of aniline to azo-benzene followed by desulphurization of dibenzothiophene (DBT) to dibenzothiophene sulfone (DBTSO). It is observed with the WO_x supported catalyst, the nature of support has a strong influence on the activity of WO_x nanoparticle. Whereas, WO_x on MCN_x proved very active and selective catalyst for the formation of azo-benzene via oxidation of aniline as well as dibenzothiophene sulfone from dibenzothiophene; compare to that WO_x on activated carbon or SBA-15 doesn't shows comparable active. These multifunctional hybrid catalysts retain their structural framework even after the reaction, and they were recovered easily from the reaction mixture through filtration and reused several times without a significant degradation in activity. Moreover, there was no contribution from leached active species in the activity and conversion was possible only in the presence of multifunctional catalyst.

Introduction

Synthesis of important oxygen containing chemicals and intermediates via ecological and economical route is one of key scientific challenges in current industrial scenario. Most of the bulk chemicals and fine speciality chemicals are synthesised by using homogenous catalyst and traditional process.¹ These established processes suffer from the use of hazardous reagents in stoichiometry and generate a large amount of waste to the environment. Heterogeneous catalysis offers a distinct advantage over homogeneous catalyst for facile catalyst separation and recycling, which further meets the requirement of green and sustainable chemistry.² Many efforts have been in last few decades to use green oxidant like O₂ and H₂O₂ along with heterogeneous catalyst to convert conventional processes to environmentally friendly technologies. Nevertheless, a very limited success has been achieved by till date due to poor efficiency and stability of heterogeneous catalyst systems in the reaction medium in presence of various oxidants.³ Therefore, there is ample scope to develop an efficient and stable heterogeneous catalyst system for industrial applications. Mesoporous carbon materials are specifically important for its potential as ORR catalysts as they are environmentally sustainable, cost-effective, and highly durable and its unique structural properties, such as high surface area, tunable pore

sizes, chemical and mechanical stability.⁴ A variety of carbon materials e.g. carbon nanotubes, activated carbon etc. have been prepared till date and has been successfully used in heterogeneous catalysis.⁵ Recently nitrogen functionalized carbon materials have been shown to have high catalytic bifunctional activity in the photocatalysis, oxygen reduction reaction, organic transformations, and semiconductors.⁶ It has also been reported that carbon nitride material are promising metal free catalyst and catalyst support in different hydrogenation and oxidation reaction.⁷

The basicity of the material was achieved by pyridine type N, which reside within the CN_x framework.⁸ For low temperature catalytic application the acid-base property of the material need to tune further by the addition of transition like tungstate to the CN_x framework. In this particular, our idea was to develop a heterogeneous carbon based tungstate catalyst that can display high activity for a variety of oxidant process like epoxidation of alkenes, alcohol oxidation, oxidative coupling of amines and oxidative desulfurization reaction. Example can be found in our previous report,⁹ where we have shown acid-base cooperative catalysis using WO_x embalmed CN_x material.

Selective formation of aromatic azo compounds through oxidative coupling of aniline is an industrially important process because aromatic azo compound are high value chemical which are widely used in industry as dyes, pigments,

food additive and drugs.¹⁰ Previously variety of oxidizing agent like MnO,¹¹ Hg (OAc)₂,¹² BaMnO₄¹³ and per acetic acid¹⁴ are used for aryl amine oxidation. Nevertheless, this process generate a large amount of inorganic waste. Now a days different metal based (Pd,¹⁵ CuCr₂O₃,¹⁶ Ag/WO₃¹⁷) heterogeneous catalyst has been applied azo compound formation. Even Au/TiO₂ has also been reported to carry out aromatic azo compound formation from aryl amine.¹⁸ Oxidative desulfurization is an industrially important and alternative process to hydrodesulphurization.¹⁹ Selective oxidation of organic sulfide to corresponding sulfide and sulfone use to decrease sulfur content from fuels and industrial effluent.²⁰ Recently Wei et.al reported Carbon nanotube as efficient catalyst for oxidative desulfurization of dibenzothiophene.²¹ The corresponding sulfides or sulfoxides are used as fine chemicals, pharmaceuticals and as valuable intermediates for the construction of chemically and biologically active molecules. Oxidative desulfurization reactions are mainly carried out over a variety of tungsten based complexes.²² Zhang et.al has also reported the oxidation of organic sulfide over mesoporous graphitic carbon nitride material under visible light.²³

In this report, we have prepared a highly active, selective reusable heterogeneous WO_x nano cluster supported on mesoporous nitrogen enriched carbon material. The catalyst has been explored for oxidation of aromatic amine and dibenzothiophene oxidation using H₂O₂ as the mild oxidizing agent.

Experimental

Materials

Tetraethylorthosilicate (TEOS), poly (ethylene oxide)-*block*-poly(propylene oxide)-*block*-poly(ethylene oxide) triblock copolymer (Aldrich, MW avg. 5800, EO₂₀PO₇₀EO₂₀, P123), ethylene diamine (NH₂C₂H₄NH₂), sodium tungstate (NaWO₄·2H₂O) were purchased from Sigma-Aldrich Co. Ethanol, carbon tetra chloride (CCl₄), NaOH, HCl, NH₃ solution were purchased from Merck KGaA, Darmstadt, Germany. All the chemicals were used without further purification. Double distilled water was prepared with a BOROSIL[®] water distillation unit.

Catalyst preparation

SBA-15 was synthesized using tetraethylorthosilicate (TEOS) as the silica source and poly (ethylene oxide)-*block*-poly(propylene oxide)-*block*-poly(ethylene oxide) triblock copolymer (Aldrich, MW avg. 5800, EO₂₀PO₇₀EO₂₀, P123) as a structure-directing agent. In a typical synthesis, 4.0 g of P123 block copolymer was dissolved under stirring in a solution of 30.0 g of water. Then, 120.0 g of HCl (2 M) and 9.1 g of TEOS were added under stirring at 40°C. After 24 h of constant stirring, the gel composition was kept at 100 °C for 48 h without any further stirring. After cooling to room temperature, the solid product was recovered by filtering, washing, drying,

and calcining at 550 °C in order to decompose the triblock copolymer.

Hexagonally ordered mesoporous WO_x/SBA-15 was synthesized by using TEOS as a silica source and poly(ethylene oxide)-*block*-poly(propylene oxide)-*block*-poly(ethylene oxide) triblock copolymer (Aldrich, MW avg. 5800, EO₂₀PO₇₀EO₂₀, P123) as a structure-directing agent. In a typical synthesis, 4.0 g of P123 block copolymer was dissolved with stirring in a solution of 30.0 g of water and the required amounts (20 mL, 10 mL, 5 mL, 2.5 mL) of aqueous sodium tungstate solution (NaWO₄·2H₂O, 0.5 M) were simultaneously and quickly added into the mixture under vigorous stirring. After one hour 120.0 g of HCl (2 M) and then 9.1 g of TEOS were added with stirring at 40 °C. After being stirred for 24 h at 40 °C, the gel composition was kept at 100 °C for 48 h without stirring. After being cooled to room temperature, the solid product was recovered by filtering, washing, drying and calcining at 550 °C.

Mesoporous nitrogen rich carbon (WO_x/CN_x) materials were synthesized using WO_x/SBA-15 as hard template using the following procedures. 1.0 g of dehydrated WO_x/SBA-15 was treated with a mixture of 4.5 g of ethylene diamine (NH₂C₂H₄NH₂) and 11 g of carbon tetra chloride (CCl₄). The mixture was refluxed at 90 °C for 6 h. Then, the obtained solid mixture (polymer silica composite) was dried and pyrolyzed at two different temperatures (600 and 800 °C) for 6 h under inert gas atmosphere. The pyrolyzed silica/nitrogen/carbon composite was washed with 2.5% wt of NaOH solution in ethanol water (1:1) mixture with vigorous stirring at 90 °C for 3 h to remove the silica framework. The process has been repeated two times. Then, the product was filtered and washed with water ethanol mixture until the filtrate had a pH value of 7.0 and dried.

Catalyst characterization

The prepared mesoporous nitrogen rich carbon materials were characterized by N₂ physisorption measurements at 77 K using an Autosorb 1C setup (Quanta chrome) adsorption analyzer. Prior to the measurements, the samples were degassed under vacuum (1×10⁻⁵ Torr) for 2 h at 200 °C. The BET specific surface areas were determined from the adsorption data in the relative pressure (P/P₀) range from 0.06 to 0.2. The pore size distributions (PSDs) were calculated from the nitrogen adsorption branch using the Barrett–Joyner–Halenda (BJH) method and the maximum of the PSD was considered as the average pore size. The pore volume was considered as the volume of liquid nitrogen adsorbed at P/P₀ = ca. 1

Morphology of the WO_x/MNC_x materials synthesised at different temperatures and different loadings of tungsten were investigated using SEM (FEI Quanta 3D) & HRTEM. Scanning electron microscopy (SEM) images were taken on a FEI Quanta 200 F instrument, using tungsten filament doped with lanthanum hexaboride (LaB₆) as an x-ray source, fitted with an ETD detector with high vacuum mode using secondary electrons and an acceleration tension of 10 or 30 kV. Images were recorded at various magnifications. All the Samples were analyzed by spreading them on

a carbon tape and coated with gold to increase the electrical conductivity. Energy dispersive X-ray spectroscopy (EDX) was used in connection with SEM for the elemental analysis. The elemental mapping was also collected with the same spectrophotometer. A JEOL JEM 2100 high-resolution transmission electron microscope (HRTEM) was employed to see porous nature of material. Samples are mounted by dispersing on ethanol on a lacey carbon Formvar coated Cu grid.

Low and wide angle powder X-ray diffractograms (XRD) were obtained with a D8-Advance-Bruker-AXS diffractometer (Cu- $K\alpha$ radiation; $\lambda = 1.5418 \text{ \AA}$) in θ - 2θ geometry and a position sensitive detector (capillary technique, thickness: 1 mm).

X-ray photoelectron spectroscopy (XPS) measurements were carried out in an ultra-high vacuum (UHV) set-up equipped with a monochromatic Al K_{α} X-ray source ($h\nu = 1486.6 \text{ eV}$), operated at 14.5 kV and 35 mA, and a high resolution Gamma data-Scienta SES 2002 analyzer. The base pressure in the measurement chamber was maintained at about 7×10^{-10} mbar. The measurements were carried out in the fixed transmission mode with pass energy of 200 eV, resulting in an overall energy resolution of 0.25 eV. A flood gun was applied to compensate the charging effects. Resolution spectra for C 1s, O 1s, and N 1s were recorded. The binding energy scales were re-calibrated based on the sp^2 hybridized C 1s line from graphitic carbon at 284.5 eV. The Casa XPS software²⁴ with a 70:30 Gaussian-Lorentzian product function and Shirley background subtraction was used for peak deconvolution. The obtained spectra from different elements were plotted using the same intensity scale for all the analyzed samples to facilitate comparison. Temperature programmed desorption (TPD) experiments were carried out in a Micromeritics, Auto Chem II 2920 instrument connected with a thermal conductivity detector (TCD) The amount and strength of the acid site were measured by ammonia adsorption-desorption technique using the same Micromeritics, Auto Chem II 2920 instrument. About 0.1 g sample was saturated with NH_3 at 100°C and flashed with He to remove the physically adsorbed NH_3 , finally the decomposition of NH_3 was carried at a heating rate of 10°C/ min under, He flow.

Multifunctional activity

The oxidation reaction was carried out in a 100ml two necked round bottom glass reactor fitted with two condenser on a hot plate with magnetic stirring (SI analytical). The reaction product was identified by GC-MS (HP 5890 GC coupled with 5972 MSD) equipped with CP-SIL-5 capillary column. The identified product was analysed in an Agilent 7890, fitted with a HP-5 (30m X 0.28mm i.d., 0.25 μm film thickness) capillary column and a FID detector. The conversion and selectivity was measured using chlorobenzene an internal standard and followed by their individual calibration curve. The activity of the catalyst was calculated as:

$$\text{Conversion (C\%)} = \frac{\text{Moles of reactant reacted (C\%)}}{\text{Moles of reactant initially used (C\%)}} \times 100$$

$$\text{Selectivity (C\%)} = \frac{\text{Moles of product (C\%)}}{\text{Moles of reactant reacted (C\%)}} \times 100$$

Results and discussion

The low angle XRD patterns of nitrogen rich carbon material are shown in Figure 1a. The XRD pattern of MCN_x reflects one prominent peak at 0.75° corresponds to the (100) plane of hexagonal $p6mm$ space group. Notably, the XRD pattern is well coincide to the XRD pattern of the ordered hexagonal mesoporous SBA-15 material.²⁵ Whereas the wide angle XRD of WO_x/MCN_x catalyst shows peak at around 25° assigned for graphitic carbon; no peak assigned for any WO_x species is observed which implicate the presence of WO_x species in nanocluster form (Fig.S1 ESI†). The 2D hexagonal structure of samples prepared at was confirmed by HRTEM (see Figure 2a-d). In the case of the sample prepared using ethylene diamine as a source of carbon & nitrogen and SBA-15 as template with 5% W loading, TEM micrograph indicated that the pores were channel-like and their arrangement were similar to that for 2D hexagonal(honeycomb) structure, however with some imperfections. The homogeneity to distribution pattern of tungsten has been confirmed by the elemental analysis facility associated with the SEM instrument and shown in Figure S2, ESI†. Finally, TEM images for the sample prepared with 2.5% WO_x loaded SBA-15 i.e. WO_x/MCN_x (2.5) showed (Figure 3c-d) regular channels and homogeneously distributed pores with a wide distribution of sizes. Both MCN_x and WO_x/MCN_x (5) show type IV N_2 adsorption/ desorption isotherm with a hysteresis loop H1 at relative pressure in the range of 0.40-0.92 as shown in Figure 1b. The pore size distribution for the MCN_x shows the mesopores at a diameter of 3.86 nm (Figure 1c) along with a pore volume of 0.61 cc g^{-1} . The specific surface area (Table S1)estimated for MCN_x was 457 $\text{m}^2 \text{g}^{-1}$ and while for the WO_x/CN_x (5) a decrease in the surface area (427 $\text{m}^2 \text{g}^{-1}$) as well as in pore volume were noticed. The pore volume decreased from to 0.61 cc g^{-1} to 0.36 cc g^{-1} , indicating the incorporation of WO_x inside the mesoporous MCN_x network.

Figure 1d shows the Raman spectra characteristics of our prepared WO_x/CN_x material. The existence of amorphous type MCN_x network can be confirmed by the low peak area ratio of G-band to D-band. The vibration frequency of MCN_x network are expected to come closer to the modes of analogous unsaturated CN molecules which are 1500-1600 cm^{-1} from chain like molecule and 1300 -1600 cm^{-1} for ring like molecule.²⁶ The signal at about 1598 cm^{-1} is attributed to the G-band of the tangential mode of graphite-like materials while the peak at around 1365 cm^{-1} is the D-band representing defects in the graphite structures.²⁷ It is been well observed, that the position

of the G-band can vary between 1500 cm^{-1} and 1600 cm^{-1} ; and in case of sp^2 bonded amorphous C, the G-mode is around 1520 cm^{-1} (lower than graphite mainly due to bond angle distortions). However, the G-band moves up with increasing sp^3 bonding in tetrahedral amorphous -C ($\geq 1595\text{ cm}^{-1}$).²⁸ This indicates a little distortions in G-D region between the bands because of special arrangement of C or N atom.

The X-ray photoelectron (XP) spectra for C 1s have been performed in order to determine the local environment of C in the MCNx network. The deconvoluted C 1s spectra (Figure 3a) show five individual peaks; on which the major two peaks at 283.9 eV and 284.8 eV are assigned to sp^2 hybridized graphite-like carbon (C-C sp^2) and sp^3 hybridized C-C sp^3 carbon shouldered with sp^2 hybridized C-N atom.⁹ Rest of the peaks can be assigned to the surface oxygen group as -CO (286.4 eV), -C=O (288.2 eV) and -C-OO (289.5 eV) respectively. The local environment of nitrogen atom also been determined by N 1s XP-spectra (Figure 3b), which on deconvolution shows three individual peaks. The fast N 1s peak at 398.5 eV assigned pyridine nitrogen (N-py), while the peak at around 401.2 eV can be assigned to N of the C-N-C network of the graphitic ring. However, the shouldered peak at 399.9 eV has been assigned to nitrogen bonded sp^2 hybridized (Nb) and nitrogen bonded to carbon atom in a terminal -C≡N group (Nt).²⁹ Total acidity of the samples were measured using NH_3 -TPD (Fig.S3 ESI†). The TPD pattern shows strong band in temperature between 150-500°C region with total number of acidic sites 0.405 mmol/g (5%WOx/MCNx) and 0.260 mmol/g (2.5 WOx/MCNx).

C-C coupling of aniline

The bi-functional reactivity of the catalyst has been tested in oxidative desulphurization as well as aniline coupling reaction. Selective oxidation of aniline to aromatics azo-compounds has been carried out with WOx/MCNx catalyst and shown in Table 1. Experimental result shown that with MCNx, oxidation of aniline is negligible (entry 2) and WOx support catalyst (entry 4-6) shows significant amount of conversion. It is assumed that during the reaction, single e^- oxidation of aniline took place to form radical cation, which exclusively mediated by the WOx/MCNx catalyst through providing unsaturated W sites. This abstraction then followed by the coupling of aniline radical cation with neutral aniline to form azo-benzene.¹⁸ The results clearly demonstrate that tungstate plays an important role in the catalytic process. As observed with the WOx supported catalyst, the nature of support has a strong influence on the activity of WOx nanoparticle. Whereas, WOx on MCNx proved to be active and selective catalyst for the formation of azo-benzene (2b); however, WOx on pure carbon (entry 2) or SBA-15 (not shown) is not found to be active under present reaction conditions. It is also observed that upon loading of WOx in MCNx network the activity and selective took positive shift however, selectivity goes down as loading go beyond 5%, which may be because of the higher particle size due to higher loading.

The effect of reaction temperature has been studied and found the catalyst can effectively convert 70.1% aniline within 12 h with 74.2% azo-benzene selectivity (Figure 4a) at a reaction temperature of 70°C. Increasing the temperature from 80°C to 90°C leads to decrease in azo-benzene selectivity from 86.5% to 83.7%, with the formation of nitroso-benzene and azoxy benzene as by-products (Figure 4a). In a longer reaction time span of 18 h at 90°C (in Figure 4b) leads to a decrease in azo-benzene selectivity to 20%, as 75.1% of the excessive oxidation product (azoxy-benzene) was formed with 89% aniline conversion. This trend is decreased for 6 & 9 h reaction time, but selective toward azo-benzene gone down, whereas nitroso-benzene came as the major with 66.3% and 21.1%. Hence, it can be assumed that nitrobenzene is the key intermediate for the formation of azo-benzene, which is been converted to azoxy-benzene (over oxidation product) with prolonged reaction time.

Aniline conversion took almost two fold increase (in Figure S4, ESI†) from 43.7% to 81.5% with the addition of doubled H_2O_2 (2 ml, 30 wt. % in H_2O). Moreover, the selectivity of azo-benzene also been found to be doubled (from 31.1% to 67.4%) whereas the selectivity of nitroso-benzene has been decreased. The observation is well concomitant to our previous results that the nitroso-benzene formed during the reaction (intermediate) and been consumed to form azo-benzene. WOx/MCNx catalyst shows maximum conversion with highest azo-benzene selectivity of 83.7% with 3 ml of H_2O_2 . Under optimized reaction condition with 3 ml of oxidant the highest H_2O_2 efficiency (24.0) can be achieved for the formation of azo-benzene (Table 1, entry 6).

Oxidative desulphurization of DBT

Oxidative desulphurization of dibenzothiophene has been carried out WOx/MCNx material and result are shown in Table 2, with WOx/MCNx (5) catalyst the conversion of DBT was 100% within 2 h and the selectivity of DBTSO (confirmed by GC-MS data shown in Figure S5, ESI†) was 99.8% at a reaction temperature of 100°C, with small amounts of DBTS (0.2%) remain as unconverted intermediate product (entry 7), indicating the effectiveness of WOx/MCNx material in oxidative desulphurization of DBT. Compare to WOx/MCNx other catalyst (entry 2-5) shows nominal activity with poor DBTSO selectivity. with the increase of tungsten loading from 1 to 5 wt% the conversion of DBT reaches 100% from 26.0% for WOx/MCNx (1) with a steady increase in DBTSO selectivity (entry 6-8), indicating that acidic site provided by tungstic oxide is essential for better conversion and DBTSO selectivity. The catalyst been reused; no such loss in activity and selectivity has been counted even after 3 successive reuse (entry 10).

The effect of reaction temperature for oxidative desulphurization was shown in Figure 4c; the conversion gradually increases up-to 100% with rise of reaction temperature from 60°C to 100°C. However, selectivity towards DBTSO has been found 95.5% at 60°C which goes to a maximum of 99.8% at 100°C after 2 h time-on-stream. Although, there is no change has been observed in the

conversion level with the increase of H_2O_2 at 100°C (in Figure S6, ESI†). The selectivity of DBTS gradually goes down to $< 8\%$ with 3 ml of (1:3 reactant to H_2O_2 ratio) H_2O_2 which was 68.1% with 2 ml H_2O_2 . So sufficient oxidant was necessary for the second step oxidant of DBTS to DBTSO. With higher amount (1:5) of H_2O_2 no much change in product distribution was observed. When the reaction is kept for 2 h (Figure 4d) the selectivity of DBTSO was found almost 100%.

To check the durability of the catalyst we have tested time-on-stream studies and shown in Figure 4d. We found 95.2% DBT conversion within 30 min time-on-stream which reaches 100% with 1 h. Furthermore, a gradual increase in DBTSO selectivity has been experienced with the time-on-stream and 100% conversion was noted within 2 h of reaction. We have utilized Sheldon's³⁰ hot filtration test which involves filtration of the catalyst part way through the reaction, followed by continuation of the reaction in absence of the catalyst. The result shows no further reaction in absence of catalyst after filtration, additionally the hot filtrate was subject for ICP analysis. The test shows a negligible presence of W in ppb level which also proves the heterogeneity of the working catalyst. WO_x species play an important role in this reaction; in presence of peroxide this WO_x species preferentially form metal-peroxo complex.^{31,32} The formation of metal-peroxo complex has been facilitated by the polar solvent especially by acetonitrile as suggested by Nizova et al.³³ now this solvent-peroxometal complex is highly active and has very short live span. Finally it transfers oxygen to the activated reactant which then goes to the product through an anionic intermediate as shown in Scheme S1 ESI†. This anionic intermediate gets stabilized by the donation of proton from polar solvent. Along with this, rate of oxygen transfer from metal-peroxo complex to the activated specie may be increased with the surface acidity.

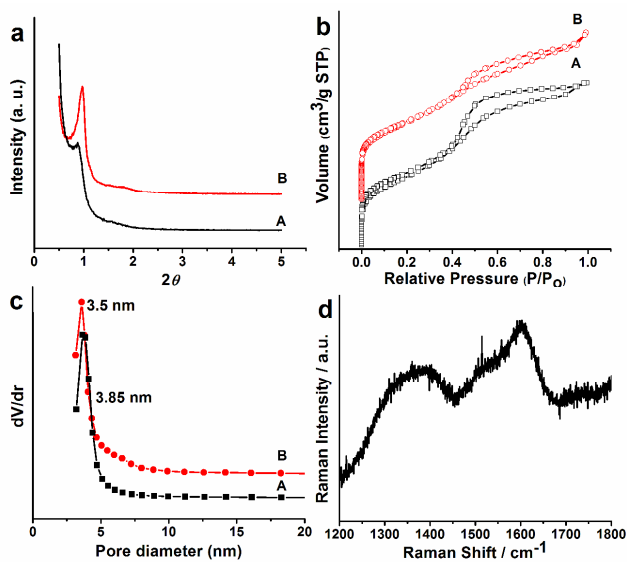


Figure 1. (a) Small-angle X-ray diffraction patterns; (b) N_2 Adsorption-desorption isotherm; (c) Pore size distribution of

(A) MCN_x and (B) WO_x/MCN_x (5) material. (d) Normalized Raman spectra of WO_x/MCN_x material with a 488 nm laser.

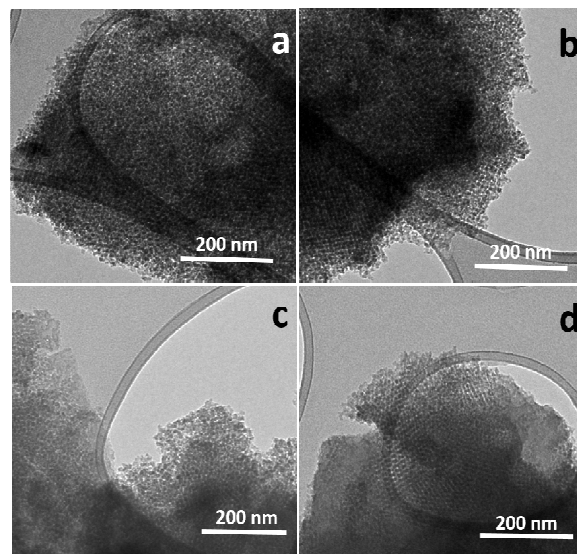


Figure 2. HRTEM images of WO_x/MCN_x (5) material synthesized with: using ethylene diamine as a source of carbon & nitrogen and 5% $\text{WO}_x/\text{SBA-15}$ as solid template.

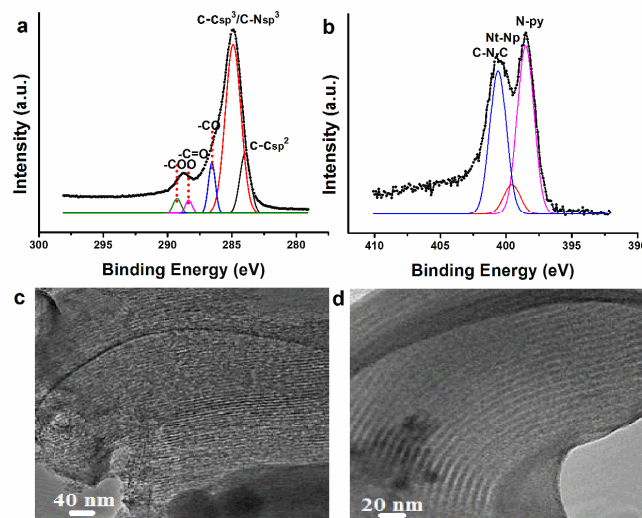


Figure 3. X-ray photoelectron spectra of (a) C 1s and (b) N 1s of WO_x/MCN_x material. (c-d) is the HRTEM images of WO_x/MCN_x (2.5).

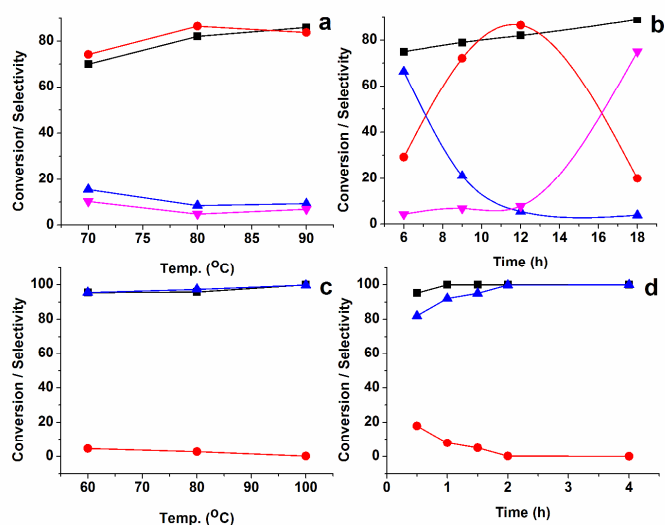


Figure 4. Effect of temperature (a) and time-on-stream (b) as a function aniline conversion and product selectivity. (■) conversion of aniline; (●) selectivity of azo-benzene; (▲) selectivity of nitroso-benzene and (▼) selectivity of azoxy-benzene. Whereas, effect of temperature (c) and time-on-stream (d) as a function of DBT conversion and product selectivity. (■) conversion of DBT; (●) selectivity of DBTS and (▲) selectivity of DBTSO.

Table 1. Selective oxidation of aniline to aromatics azo-compounds over various carbon based catalyst.

Sl No.	Catalyst	C _{Aniline}	Selectivity			E _o
			S _{2b}	S _{2c}	S _{2d}	
1	Blank	-	-	-	-	-
2	MCN _x	~1.9	13.5	16.2	70.3	~0.1
3	WO _x /C	-	-	-	-	-
4	WO _x /CN _x (1)	33.6	67.4	11.7	20.9	7.5
5	WO _x /CN _x (2.5)	57.8	73.7	8.7	17.6	14.2
6	WO _x /CN _x (5)	86.1	83.7	9.3	6.9	24.0
7	WO _x /CN _x (10)	89.7	79.5	14.5	7.0	23.7
8	WO _x /CN _x (5) ^e	81.9	83.9	9.4	6.7	22.9

0.93 g (10 mmol) aniline, 10 ml CH₃CN, 0.05 g catalyst, temperature-90°C, and time-12 h, E_o: H₂O₂ efficiency calculated by (100 x moles of **2b** formed) / total moles of H₂O₂ added. C_{aniline}= conversion of aniline, S_{2b}=selectivity of **2b**, e = after 3 reuse, S_{2c}=selectivity of **2c** and S_{2d}=selectivity of **2d**.

Table 2. Oxidative desulphurization of DBT over carbon based catalyst.

Sl No.	Catalyst	C _{DBT}	Selectivity		E _o
			S _{1b}	S _{1c}	
1	Blank	2.7	98.5	1.5	0.003
2	SBA-15	31.0	79.8	20.2	0.5
3	WO _x /SBA-15	47.9	46.6	51.6	2.2
4	MCN _x	22.1	41.2	58.8	1.2
5	WO _x /C	41.2	75.9	24.1	0.9
6	WO _x /CN _x (1)	26.0	21.1	78.9	1.8
7	WO _x /CN _x (2.5)	66.1	13.8	86.2	5.1
8	WO _x /CN _x (5)	100	0.2	99.8	9.0
9	WO _x /CN _x (5) ^a	~99.9	0.7	99.3	8.9

0.5 g (2.7 mmol) Dibenzothiophene(DBT), 10 ml CH₃CN, 0.05 g catalyst, temperature-100°C, time-2h, ^a after 3 reuse, E_o: H₂O₂ efficiency calculated by (100 x moles of DBTSO formed) / total moles of H₂O₂ added. S_{1b}=selectivity of DBTS and S_{1c}=selectivity of DBTSO.

Conclusions

2D hexagonal mesoporous nitrogen-rich carbon materials embedded with highly dispersed WO_x nanocluster were prepared through a novel approach taking WO_x supported SBA-15 as a hard template. The newly synthesized materials were found to be excellent bifunctional carbon nitride-based catalyst systems for selective oxidation of aniline to aromatics azo-compounds as well as oxidative desulphurization of dibenzothiophene.

From the results of the present study, it should be possible to develop a wide array of metal embedded MCN_x material for selective oxidation, provided that enough metal dispersion and defect sites are generated on the surface. However, WO_x/MCN_x not only gives the highest selectivity of the materials tested here but also should allow the efficient one-pot conversion of aniline into azo-compounds as well as dibenzothiophene into dibenzothiophene sulfone.

Acknowledgements

R.G. acknowledges the Council for Scientific and Industrial Research (CSIR), India, AB gratefully acknowledges DST for fast track grant. We also acknowledge the Director CSIR-IIP for his support. The authors thank the Analytical Science Division, Indian Institute of Petroleum, for analytical services.

Notes and references

^a R. Goyal, L. N. Sivakumar Konathala, M. Pandey, Dr. A. Bordoloi Refinery Technology Division CSIR-Indian Institute of Petroleum Dehradun-248005, UK, (India) Tel.: +91 135 2525898; Fax: +91 135 2660202 E-mail: ankurb@iip.res.in

^b Deepa Dumbre Centre for Advanced Material and Industrial chemistry, School of Applied Sciences,

University of Melbourne, Australia 3000.

†Electronic Supplementary Information (ESI) available: See DOI: 10.1039/b000000x/

1. a) R. A. Sheldon, M. Wallau I. W. C. E. Arends and U. Schuchardt, *Acc. Chem. Res.*, 1998, **31**, 485.; b) A. Corma and H. Garcia, *Chem. Rev.* 2003, **103**, 4307.
2. Y. M. A. Yamada, C. K. Jin and Y. Uozumi, *Org. Lett.*, 2010, **12**, 4540.
3. a) M. Lamblin, L. Nassar-Hardy, J. C. Hierso, E. Fouquet and F.X. Felpin, *Adv. Synth. Catal.*, 2010, **352**, 33; b) T. Mitsudome, A. Nougima, T. Mizugaki, K. Jitsukawa and K. Kaneda, *Adv. Synth. Catal.* 2009, **351**, 1890; c) G. Maayan and R. Neumann, *Catal. Lett.* 2008, **123**, 41; d) P. Sarmah, R. Chakrabarty, P. Phukan and B. K. Das, *J. Mol. Catal. A: Chem.*, 2007, **268**, 36.; e) K. Ebitani, K. Motokura, T. Mizugaki and K. Kaneda, *Angew. Chem., Int. Ed.*, 2005, **44**, 3423.
4. W. Yang, T. P. Fellingner, and M. Antonietti, *J. Am. Chem. Soc.*, 2011, **133**, 206.
5. a) F. R. Reinoso, *Carbon*, 1998, **36**, 159; b) P. Serp, M. Corrias and P. Kalck, *Appl. Catal. A*, 2003, **253**, 337; c) P. Serp and J. L. Figueiredo, in *Carbon Materials for Catalysis*, John Wiley & Sons Inc., Hoboken, NJ, USA, 2009.
6. a) C. N. Tharamani, A. Bordoloi, W. Schuhmann and M. Muhler, *ChemSusChem* 2012, **5**, 637; b) F. Su, S. C. Mathew, S. Blechert, G. Lipner, X. Fu, X. Wang and M. Antonietti, *J. Am. Chem. Soc.*, 2010, **132**, 16299.
7. H. Wang, Y. Gong and Y. Wang, *RSC Adv.*, 2014, **4**, 45753.
8. X. Jin, V. V. Balasubramanian, S. T. Selvan, D. P. Sawant, M. A. Chari, G. Q. Lu, and A. Vinu, *Angew. Chem. Int. Ed.*, 2009, **48**, 7884.
9. R. Goyal, B. Sarkar, N. Lucus and A. Bordoloi, *ChemCatChem*, 2014, **6**, 3091.
10. a) R. Egli, A. P. Peter and H. S. Freeman, in *Colour Chemistry: The Design and Synthesis of Organic Dyes and Pigments*, Eds. (Elsevier, London, 1991, chap. VII); b) S. C. Catino and E. Farris, in *Concise Encyclopedia of Chemical Technology* (Wiley, New York, 1985); c) K. Venkataraman, in *Chemistry of Synthetic Dyes* (Academic Press, London, 1970, chap. VI).
11. O. H. Wheeler and D. Gonzalez, *Tetrahedron*, 1964, **20**, 189.
12. E. Wenkert and B. Wickberg, *J. Am. Chem. Soc.*, 1962, **84**, 4914.
13. H. Firouzabadi and Z. Mostafavipoor, *Bull. Chem. Soc. Jpn.* 1983, **56**, 914.
14. R. W. White and W. D. Emmons, *Tetrahedron*, 1962, **17**, 31.
15. L. Hu, X. Cao, L. Shi, F. Qi, Z. Guo, J. Lu, and H. Gu, *Org. Lett.*, 2011, **13**, 5640.
16. S. S. Acharyya, S. Ghosh, and R. Bal, *ACS Sustainable Chem. Eng.*, 2014, **2**, 584.
17. S. Ghosh, S. S. Acharyya, T. Sasaki and R. Bal, *Green Chem.*, 2015, **17**, 1867.
18. A. Grierrane, A. Corma and H. Garcia, *Science*, 2008, **322**, 1661.
19. a) A. Rabion, F. Fajula, J. R. Bernard and V. Hulea, US Patent 0,102,252 (2003); b) W. Gore, S. Bonde, G.E. Dolbear and E.R. Skov, US Patent 20,020,035,306 (2002); c) F. Figueras, J. Palomeque, S. Loridant, C. Feche, N. Essayem and G. Gelbard, *J. Catal.* 2004, **226**, 25.
20. M. R. Maurya, A. Arya, A. Kumar, M. L. Kuznetsov, F. AVECILLA, and J. C. Pessoa, *Inorg. Chem.* 2010, **49**, 6586.
21. W. Zhang, H. Zhang, J. Xiao, Z. Zhao, M. Yu and Z. Li, *Green Chem.*, 2014, **16**, 211.
22. S. P. Das, J. J. Boruah, H. Chetry and N. S. Islam, *Tetra. Lett.* 2012, **53**, 1163.
23. P. Zhang, Y. Wang, H. Li and M. Antonietti, *Green Chem.*, 2012, **14**, 1904.
24. N. Fairley, Casa XPS Version 2.3.15, copyright 1999-2009 Casa Software Ltd.
25. S. Liu, H. Zhang, X. Meng, Y. Zhang, L. Ren, F. Nawaz, J. Liu, Z. Li and F. Xiao, *Micro. Meso. Mater.* 2010, **136**, 126.
26. A. C. Ferrari, S. E. Rodil and J. Robertson, *Phys. Rev. B* 2003, **67**, 155306.
27. D. Roy, M. Chhowalla, N. Hellgren, T. W. Clyne and G. A. J. Amaratunga, *Phys. Rev. B*, 2004, **70**, 035406.
28. S. E. Rodil, A. C. Ferrari, J. Robertson and W. I. Milne, *J. Appl. Phys.*, 2001, **89**, 5425.
29. a) N. Fairley, Casa XPS Version 2.3.15, copyright 1999-2009 Casa Software Ltd.; b) C. D. Wagner, W. M. Riggs, L. E. Davis, J. F. Moulder and G. E. Muilenberg, *Handbook of X-ray Photoelectron Spectroscopy*, PerkinElmer Corp., Eden Prairie, USA, 1979.
30. H. E. B. Lempers and R. A. Sheldon, *J. Catal.*, 1998, **175**, 62.
31. X. Wang, J. Wu, M. Zhhao, Y. Lv, G. Li and C. Hu, *J. Phys. Chem. C*, 2009, **113**, 14270.
32. M. K. Chaudhuri and S. K. Ghosh, *J. Chem. Soc., Dalton Trans.*, 1984, **507**.
33. G. V. Nizova, Y. N. Kozlov, and G. B. Shulpin, *Russian Chemical Bulletin, International Edition*, 2004, **53**, 2330.